Research Square

Preprints are preliminary reports that have not undergone peer review.
They should not be considered conclusive, used to inform clinical practice,
or referenced by the media as validated information.

Modulation of Indonesian Throughflow transport by the Madden-Julian Oscillation across ENSO and IOD phases in the Makassar Strait

Fadli Syamsudin

fadl001@brin.go.id

National Research and Innovation Agency (BRIN)

Naokazu Taniguchi

Hiroshima University

Mega L Syamsuddin

Universitas

Sopia Lestari

National Research and Innovation Agency (BRIN)

Indah H. Lizar

Universitas

Yusuf S. Djajadihardja

National Research and Innovation Agency (BRIN)

Research Article

Keywords: Indonesian Throughflow, Madden-Julian Oscillation, El Niño-Southern Oscillation (ENSO), Indian Ocean Dipole (IOD), thermocline transport variability, ocean-atmosphere interaction, tropical inter-basin exchange

Posted Date: November 10th, 2026

DOI: https://doi.org/10.21203/rs.3.rs-11418055/v1

License: This work is licensed under a Creative Commons Attribution 4.0 International License.
Read Full License

Additional Declarations: No competing interests reported.

Modulation of Indonesian Throughflow transport by the Madden-Julian Oscillation across ENSO and IOD phases in the Makassar Strait

Fadli Syamsudin[a]*, Naokazu Taniguchi[b], Mega L Syamsuddin[c], Sopia Lestari[a], Indah H. Lizar[c], Yusuf S. Djajadihardja[a]

[a]National Research and Innovation Agency (BRIN), Jalan M.H. Thamrin 8, Jakarta, Indonesia

[b]Graduate School of Advanced Science and Engineering, Hiroshima University, Higashi-Hiroshima, Japan

[c]Department of Marine Sciences, Faculty of Fisheries and Marine Sciences, Universitas Padjadjaran. Jl. Raya Bandung Sumedang KM 21, West Java, Indonesia

*_Corresponding author:_ Fadli Syamsudin, fadl001@brin.go.id, ORCID: 0009-0006-4489-3244

ABSTRACT

The Indonesian Throughflow (ITF) is the principal low-latitude ocean gateway linking the Pacific and Indian Oceans, and its variability contributes to inter-basin redistribution of heat and freshwater. Although seasonal and interannual variability of the ITF is well documented, the extent to which intraseasonal forcing interacts with the background climate conditions remains insufficiently quantified. Here we investigate the modulation of Makassar Strait ITF variability by the Madden-Julian Oscillation (MJO) under concurrent El Niño-Southern Oscillation (ENSO) and Indian Ocean Dipole (IOD) conditions. Daily 1/12° GLORYS12 reanalysis fields for 2004-2020 are evaluated against INSTANT mooring observations and used to construct strong MJO phase composites of circulation and transport. The results show clear phase-dependent intraseasonal variability. Surface currents generally strengthen during suppressed MJO phases and weaken during active phases, with seasonal dependence in the magnitude and depth of the response. The largest transport variability occurs within the thermocline, with values at 100 m reaching approximately 4.7-5.0 Sv during JJA phases 1-2, while transport during other seasons and phases is generally lower. ENSO and IOD modify the MJO response in different ways. El Niño can enhance early-phase surface currents while reducing late-phase transport, whereas La Niña maintains a stronger background throughflow without proportionally increasing MJO anomalies. Positive IOD events introduce additional seasonal and phase-dependent modulation, particularly during JJA-SON. These results indicate that Makassar Strait transport variability reflects state-dependent interaction among monsoonal forcing, interannual climate modes, and intraseasonal MJO variability rather than simple linear superposition.

Keywords: Indonesian Throughflow, Madden-Julian Oscillation, El Niño-Southern Oscillation (ENSO), Indian Ocean Dipole (IOD), thermocline transport variability, ocean-atmosphere interaction, tropical inter-basin exchange.

1. Introduction

The Indonesian Throughflow (ITF) constitutes a fundamental component of the global ocean circulation system and serves as the only low-latitude interocean exchange linking the Pacific and Indian Oceans (Gordon, 1986; Sprintall et al., 2014). The ITF transfers warm, relatively fresh Pacific waters into the Indian Ocean and contributes to regional heat and freshwater redistribution, while also influencing the strength and structure of the global

thermohaline circulation (Gordon, 2005; Sprintall et al., 2014). Approximately 70% of the total ITF transport passes through the Makassar Strait, making it the principal conduit of tropical inter-basin exchange (Gordon et al., 2008). Mooring observations from 2004 to 2006 reported a mean transport of 11.6 ±3.3 Sv (1 Sv = 10^6 m^3 s^{-1}), highlighting both its magnitude and variability (Gordon et al., 2008).

ITF variability spans multiple temporal scales, including intraseasonal, seasonal, and interannual variability (Gordon et al., 2019). Its transport structure is vertically complex, with distinct surface and thermocline responses to atmospheric forcing (Song and Gordon, 2004; Susanto and Gordon, 2005). Because the Maritime Continent lies at the convergence of major tropical climate systems, the ITF is strongly influenced by coupled ocean-atmosphere processes, including the Asian-Australian monsoon, the El Niño-Southern Oscillation (ENSO), the Indian Ocean Dipole (IOD), and the Madden-Julian Oscillation (MJO) (Webster et al., 1998).

Intraseasonal variability over the Maritime Continent is dominated by the MJO, a planetary-scale eastward-propagating atmospheric disturbance with a 30-90-day periodicity (Madden and Julian, 1971, 1972; Yoneyama et al., 2008). As the convective envelope propagates across the Indonesian seas (typically phases 4-5), associated wind stress anomalies can modify sea level gradients and upper-ocean circulation. Previous studies suggest that MJO-related variability accounts for a substantial fraction of transport variations along the ITF pathway, influencing up to ~50% of variability in the outflow region and ~20% within the Makassar Strait (Tamasiunas et al., 2021). However, the mechanisms governing phase-dependent modulation, particularly during suppressed versus active MJO conditions, remain incompletely characterized.

On interannual timescales, ENSO and the IOD strongly modulate Indo-Pacific circulation. ENSO is characterized by anomalous sea surface temperature (SST) variability in the central and eastern tropical Pacific and induces large-scale changes in atmospheric convection, wind stress, and thermocline structure (Yeh et al., 2018; McPhaden et al., 2021). Westerly wind bursts associated with MJO activity can generate equatorial Kelvin waves, alter thermocline depth, and influence the onset or amplification of El Niño events (McPhaden et al., 2021; Zhang, 2005). The IOD, defined by zonal SST gradients across the tropical Indian Ocean (Nagura and McPhaden, 2010; Yang et al., 2015), is also coupled to intraseasonal variability, and IOD conditions can modulate MJO activity over the Indian Ocean and Maritime Continent

(Wilson et al., 2013). These interactions suggest that intraseasonal and interannual climate modes are dynamically linked rather than independent.

Although seasonal and interannual ITF variability are well characterized, the coupled influence of intraseasonal MJO forcing and concurrent ENSO-IOD conditions on Makassar Strait transport remains insufficiently quantified, eventually with respect to the vertical structure of transport anomalies under combined climate states and their potential for state-dependent modulation. Understanding these multiscale interactions is essential because ITF variability affects the redistribution of heat and freshwater across ocean basins and, in turn, influences global overturning circulation and tropical climate feedbacks.

Here, we investigate the coupled influence of the MJO and ENSO-IOD variability on ITF transport in the Makassar Strait using high-resolution ocean reanalysis validated against in situ observations. By examining phase-locked intraseasonal variability under different interannual climate conditions, we aim to clarify how cross-scale ocean-atmosphere interactions regulate tropical inter-basin exchange.

2. Methods

2.1 Study area and data

The study focuses on the Makassar Strait, the primary western route of the Indonesian Throughflow (ITF), which carries approximately 70% of total ITF transport (Gordon et al., 2008). Volume transport was calculated at two cross-sectional locations: (A) the northern entrance of the strait and (B) near the INSTANT mooring site at the Dewakang sill (2°51.9′S, 118°27.3′E; Gordon et al., 2008). Figure 1 illustrates the study area and the 2 (two) sites A and B, for volume transport calculation.

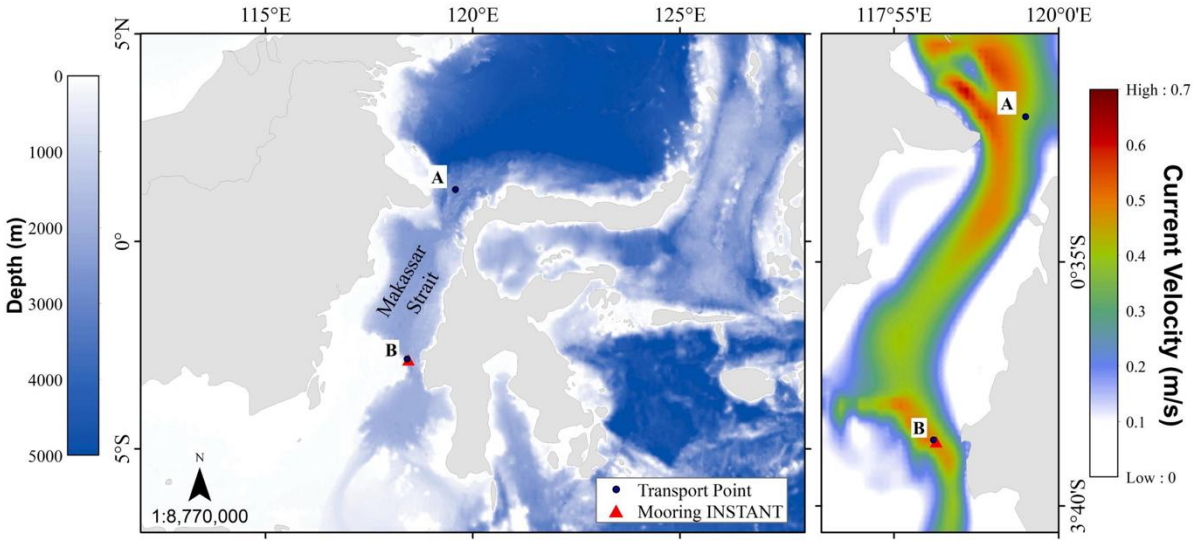


Figure 1. Study area in the Makassar Strait (MS), Indonesian waters (left). Volume transports are calculated at points A (strait entrance in the northern MS) and B (INSTANT mooring at Dewakang Sill in the southern MS) (right). The INSTANT mooring data from 2004 to 2006 at 2°51.9′S and 118°27.3′E are used to evaluate reanalysis performance.

We analysed daily data spanning 2004-2020 from the Copernicus Marine Service Global Ocean Physics Reanalysis (GLORYS12). GLORYS12 assimilates satellite and in situ observations into a high-resolution ocean circulation model to reconstruct historical ocean states (Jean-Michel et al., 2021). The dataset has a horizontal resolution of 1/12° (~9 km at the equator) and 50 vertical levels, enabling representation of mesoscale and upper-ocean variability. Previous assessments indicate that GLORYS12 reproduces seasonal and interannual variability realistically across regional scales (Jean-Michel et al., 2021; Amaya et al., 2023).

Reanalysis currents were validated against in situ observations from the International Nusantara Stratification and Transport (INSTANT) program conducted between January 2004 and November 2006 (Gordon et al., 2008; Sprintall et al., 2004). The INSTANT mooring, deployed at 2°51.9′S, 118°27.3′E, recorded current velocities at nominal depths of 50, 150, 350, and 750 m. The mooring was first deployed in January 2004, serviced in July 2005, and recovered in November 2006 (Gordon et al., 2008). These observations provide the benchmark estimate of Makassar Strait mean transport (11.6 ± 3.3 Sv).

2.2 Transport calculation and validation

Indonesian Throughflow (ITF) volume transport was calculated from the meridional current velocity in the GLORYS12 reanalysis by integrating velocity across the horizontal width and vertical thickness of the selected cross-sectional layers at locations A and B in the Makassar Strait. The transport through a layer bounded by depths (z1) and (z2) was expressed as

$$T\,(z_1, z_2, t) = \int_{z_1}^{z_2} \int_{x_1}^{x_2} v(x, z, t)\, dx\, dz$$

where T(z1,z2,t) is the volume transport through the specified layer at time (t), v(x,z,t) is the meridional velocity component, x is the horizontal distance across the section, and z is depth. The limits (x1) and (x2) represent the horizontal extent of the selected cross-section, while (z1) and (z2) are set for the upper and lower boundaries of the vertical layer, respectively. The integral was evaluated numerically using the gridded velocity data:

$$T(t) = \sum_{i=1}^{N_x} \sum_{k=1}^{N_z} v_{i,k}(t) \Delta x_i\, \Delta z_k$$

where T(t) is the volume transport at time (t), $v_{i,k}$ (t) is the meridional velocity in horizontal grid cell (i) and vertical layer (k), Delta x_i is the horizontal width of grid cell (i), Delta z_k is the vertical thickness of layer (k), and N_x and N_z are the numbers of horizontal grid cells and vertical layers included in the integration, respectively.

The horizontal grid-cell width was set to 8,333.4 m, while the vertical thickness of each model layer was obtained from the depth-dependent layer-thickness data. The depth-resolved transport profiles shown in Figures 7 and 8 were calculated over the vertical intervals of 0-25, 26-56, 56-110, 110-156, 156-200, 201-250, and 251-300 m, corresponding to nominal depths of 25, 50, 100, 150, 200, 250, and 300 m, respectively. Each value represents meridional volume transport integrated across the selected horizontal section and over the corresponding vertical interval, rather than velocity at a single depth or cumulative transport from the surface to the nominal depth. Transport was expressed in Sverdrups (Sv), where 1 Sv = 10^6 m^3 s^{-1}. Negative values indicate southward transport.

To investigate variability at different timescales, the transport time series were decomposed using Seasonal-Trend decomposition based on LOESS (STL), a non-parametric method that separates a time series into trend, seasonal, and residual components (Cleveland et al., 1990).

After removal of the seasonal component, the resulting anomalies were smoothed using a 30-day moving average to highlight intraseasonal variability.

Reanalysis performance relative to INSTANT observations was evaluated using the root mean square error (RMSE), mean absolute error (MAE), and Spearman rank correlation coefficient (ρ). RMSE and MAE quantify the magnitude of different between reanalysis and observed velocities, with RMSE assigning greater weight to larger errors. Spearman's (ρ) measures the strength and direction of their monotonic association.

2.3 Atmospheric forcing and climate indices

Daily zonal wind at 850 hPa was obtained from the ERA5 reanalysis produced by the Copernicus Climate Change Service (C3S). The 850 hPa level (~1.5 km altitude) captures lower-tropospheric circulation anomalies associated with deep convection and is widely used to monitor Madden-Julian Oscillation (MJO) activity (Wheeler and Hendon, 2004).

MJO variability was characterized using the Real-time Multivariate MJO (RMM) index (Wheeler and Hendon, 2004), obtained from the Australian Bureau of Meteorology. MJO activity was classified according to RMM amplitude and propagation phase. Days with an RMM amplitude >1 were classified as strong MJO conditions, while those with an amplitude ≤1 were classified as weak MJO conditions. The RMM index divides MJO activity into eight canonical phases representing the eastward propagation of convective anomalies (Wheeler and Hendon, 2004; Lestari et al., 2022). Only strong MJO conditions were included in the composite analyses.

Interannual climate variability was characterized using the Niño 3.4 index for ENSO and the Dipole Mode Index (DMI) for the Indian Ocean Dipole (IOD). ENSO phases were defined using the Oceanic Niño Index (ONI), based on three-month running mean SST anomalies in the Niño3.4 region (5°N-5°S, 120°W-170°W), with El Niño (La Niña) conditions identified when ONI exceeds +0.5°C (falls below -0.5°C) for at least five consecutive overlapping seasons (McPhaden et al., 2021).

IOD variability was quantified using the DMI, defined as the SST anomaly difference between the western and eastern equatorial Indian Ocean (Saji and Yamagata, 2003). Positive (negative) DMI values correspond to positive (negative) IOD events.

2.4 Composite and interaction analysis

Strong MJO days were composited by phase to evaluate phase-locked intraseasonal transport variability. The composites were further stratified by concurrent ENSO and IOD conditions to assess state-dependent modulation. The number of daily samples contributing to each composite is reported in Table 2. These counts represent phase-days rather than independent MJO events because consecutive days may belong to the same MJO episode. Statistical significance of anomalies was evaluated using two-tailed tests with autocorrelation-adjusted degrees of freedom. For Figures 3-6, only selected strong MJO phases for which spatial distributions differed significantly from the climatology at the 95% confidence level are shown, based on a statistical t-test.

3. Results

3.1 Evaluation of GLORYS12 Reanalysis with INSTANT Observations

To assess how well GLORYS12 represents Makassar Strait circulation, reanalysis meridional velocities were compared with INSTANT mooring observations during 2004-2006. The comparison was performed after removing the seasonal component using LOESS decomposition and applying a 30-day moving average to emphasize intraseasonal variability. The validation metrics in Table 1 indicate depth-dependent agreement. Mean absolute errors (MAEs) are 0.23, 0.07, 0.17, and 0.11 m s^{-1} at 50, 150, 350, and 750 m, respectively, while RMSE values are 0.28, 0.09, 0.19, and 0.12 m s^{-1}. Spearman rank correlations are 0.41, 0.50, 0.59, and -0.11, respectively. The strongest monotonic agreement occurs at 350 m, whereas the relationship at 750 m is weak and negative. These results support the use of GLORYS12 for the seasonal and intraseasonal analysis, mainly in the upper and intermediate layers, although its performance is not uniform throughout the water column.

Table 1. Validation of GLORYS12 and INSTANT current velocities using Spearman rank correlation, MAE, and RMSE.

Validation Methods	Depths (m)			
	50	150	350	750
MAE	0.23	0.07	0.17	0.11
RMSE	0.28	0.09	0.19	0.12
Spearman rank correlation coefficient (ρ)	0.41	0.50	0.59	-0.11

The 30-day moving-average time series shows broadly coherent temporal variability between GLORYS12 and INSTANT, particularly at 150 and 350 m (Figure 2). The smallest MAE occurs at 150 m, whereas the highest Spearman correlation occurs at 350 m. The larger discrepancy at 50 m and the weak relationship at 750 m indicate that reanalysis performance varies with depth, so variability in the deepest layer should be interpreted cautiously.

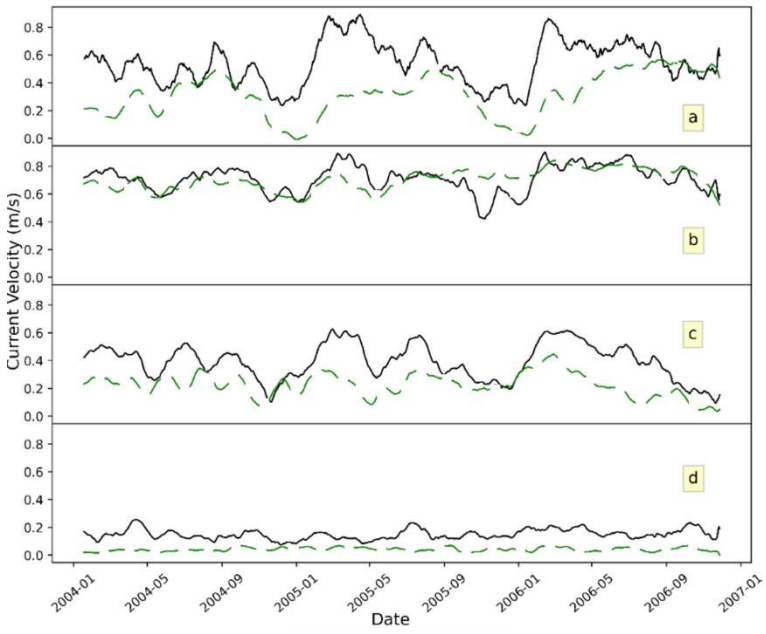


Figure 2. 30-day moving average time series of GLORYS12 (black solid line) and INSTANT current velocities (green dashed line) at 50 (a), 150 (b), 350 (c), and 750 m (d).

The smallest MAE occurs at 150 m (0.07 m s^{-1}), whereas the strongest Spearman correlation occurs at 350 m ($\rho = 0.59$). The 50-m record has the largest RMSE (0.28 m s^{-1}). At 750 m, the correlation is weak and negative ($\rho = -0.11$), indicating little monotonic correspondence between GLORYS12 and INSTANT velocities at this depth. This weak negative association should not be interpreted as evidence of a robust physical reversal, but rather as an indication that the two datasets capture the deepest-layer variability differently.

Differences between reanalysis and in-situ velocities may arise from limitations in model resolution, data assimilation, and the representation of local circulation, as well as observational uncertainty. These factors can become more consequential at depth, where flow may be influenced by complex topography and where the available observations are limited. The weak agreement at 750 m highlights the need for caution when interpreting variability in the deepest layer.

3.2 Seasonal and Intraseasonal Current Variability during MJO, ENSO and IOD Events

The number of daily samples (n) contributing to each strong Madden-Julian Oscillation (MJO) phase composite and to the corresponding composites under concurrent ENSO and IOD conditions is summarized in Table 2. These sample counts establish the sampling basis for examining seasonal and phase-dependent variability in Makassar Strait currents and for assessing how the background climate state may influence the MJO-related response.

Table 2. Number of daily samples (n) associated with strong MJO phases in each season and their co-occurrence with El Niño, La Niña, positive IOD, and negative IOD conditions during 2004-2020.

MJO Phase	Strong MJO				Strong MJO and El Niño				Strong MJO and La Niña			
	DJF	MAM	JJA	SON	DJF	MAM	JJA	SON	DJF	MAM	JJA	SON
1	66	141	285	109	11	16	46	51	26	29	52	23
2	93	114	219	110	16	16	22	56	49	19	62	30
3	105	150	63	103	45	26	9	60	27	34	18	23
4	132	122	66	149	49	26	10	69	45	25	16	36
5	167	106	66	212	53	15	9	42	71	30	13	96
6	180	99	84	88	70	7	16	19	62	32	18	45
7	208	109	66	45	76	11	15	10	82	32	6	30
8	110	159	74	91	53	32	17	29	42	39	12	38

MJO Phase	Strong MJO and Positive IOD				Strong MJO and Negative IOD			
	DJF	MAM	JJA	SON	DJF	MAM	JJA	SON
1	-	14	69	50	-	-	12	-
2	-	10	42	40	-	-	5	-
3	-	11	26	24	-	-	-	-
4	-	4	10	27	-	-	-	-
5	-	4	3	41	-	-	-	-
6	-	2	3	16	-	-	-	-
7	-	14	4	14	-	-	2	-
8	-	24	3	43	-	-	-	-

Strong MJO conditions were defined as days when the Real-time Multivariate MJO (RMM) amplitude exceeded 1 (Wheeler and Hendon, 2004). These days were assigned to one of the eight canonical MJO phases that describe the eastward progression of the MJO convective and circulation anomalies. The phases provide a framework for examining the evolution of atmospheric forcing across the Indian Ocean, Maritime Continent, and western Pacific (Wheeler and Hendon, 2004; Rauniyar and Walsh, 2011; Lestari et al., 2026). Table 2 further separates the strong-MJO samples according to the concurrent El Niño, La Niña, positive IOD, and negative IOD states, allowing the seasonal contribution and sample availability of each composite to be assessed.

The Makassar Strait circulation exhibits pronounced seasonal variability, upon which MJO activity introduces intraseasonal fluctuations. The magnitude and spatial structure of the associated current response may vary among the four seasons: December-February (DJF), March-May (MAM), June-August (JJA), and September-November (SON), and under different ENSO and IOD background conditions. The following analysis examines the seasonal and MJO-phase dependence of surface-current velocity, including its variation under concurrent ENSO and IOD conditions. The corresponding volume-transport response is described in Section 3.3.

3.2.1 Wet season (December-February/DJF)

During the wet season (DJF), the greatest changes in surface current velocity associated with strong MJO events occur near the northern entrance and central Makassar Strait (Figure 3). Comparison with the climatological mean for each MJO phase shows significant differences during phases 1, 3, and 4 (Table 3). During phase 1, the current velocity at point A decreases to 0.21 m s^{-1} compared with the climatological mean of 0.37 m s^{-1}. In contrast, during phases 3-4, the current strengthens at point B to approximately 0.40–0.45 m s^{-1}, relative to the climatological mean of 0.22 m s^{-1}. Spatially, current flow from northern Kalimantan and northern Sulawesi tends to converge toward the central Makassar Strait during phases 1-3, before turning eastward during phases 4-7. This change in direction contributes to a weakening of the current in the central strait. In addition, inflow from the Java Sea can modify the southward current within the Makassar Strait.

The surface current velocity in the central Makassar Strait is the lowest during the wet season compared with the other seasons. This seasonal condition is consistent with the influence of the Asia-Australia monsoon, during which water from the Java Sea and Pacific enters the Banda Sea, contributing to the accumulation of warm, low-salinity water and suppression of the thermocline. At this time, the Intertropical Convergence Zone (ITCZ) extends from south of Java toward northern Australia, limiting the movement of water from the Banda Sea toward the Indian Ocean. The resulting weakening of the pressure gradient between the Pacific and Indian oceans contributes to weaker flow through the Makassar Strait (Wyrtki, 1987).

The MJO also exhibits strong seasonal variability over Indonesia during the wet season (Pei et al., 2021). Previous studies have demonstrated that active MJO phases increase the probability of extreme rainfall over western and central Indonesia (Birch et al., 2016; Lestari et al., 2022; Peatman et al., 2014). Although these studies primarily addressed atmospheric precipitation, the associated atmospheric circulation changes can also influence ocean conditions. During phases 3-4, when the MJO convective center is located over Indonesia, the associated circulation can further push Java Sea waters toward eastern Indonesia and reduce the pressure gradient across the region. This promotes water accumulation near the entrance of the Makassar Strait and favors an eastward deflection of the flow. Consistent with this interpretation, Napitu et al. (2019) found that intraseasonal processes responsible for reducing

surface layer ITF transport in the Makassar Strait are more dominant during the wet season than during the dry season.

The interaction between the MJO and ENSO further modifies the current response. The MJO and ENSO are known to interact dynamically and influence one into another evolution (Zhang, 2005). During the mature stage of El Niño, for example, eastward MJO propagation can weaken, accompanied by changes in the amplitude of MJO-related zonal winds at 850 hPa (Li et al., 2023). The MJO - ENSO relationship is also dependent on the type and characteristics of the El Niño event (Pang et al., 2016).

In the present study, the spatial distributions of surface current velocity during combined MJO-ENSO and MJO-IOD events reveal substantial seasonal modulation. No IOD events occurred during the DJF period within the 2004-2020 study period. During El Niño years, the current is stronger than both the climatological mean and the strong MJO only condition. At phase 1, current velocity increases to approximately 0.50 m s^{-1} at point A and 0.45 m s^{-1} at point B. This is particularly notable because phase 1 under strong MJO conditions alone is weaker than the climatological mean. The occurrence of El Niño therefore substantially modifies the current response to the MJO during the wet season.

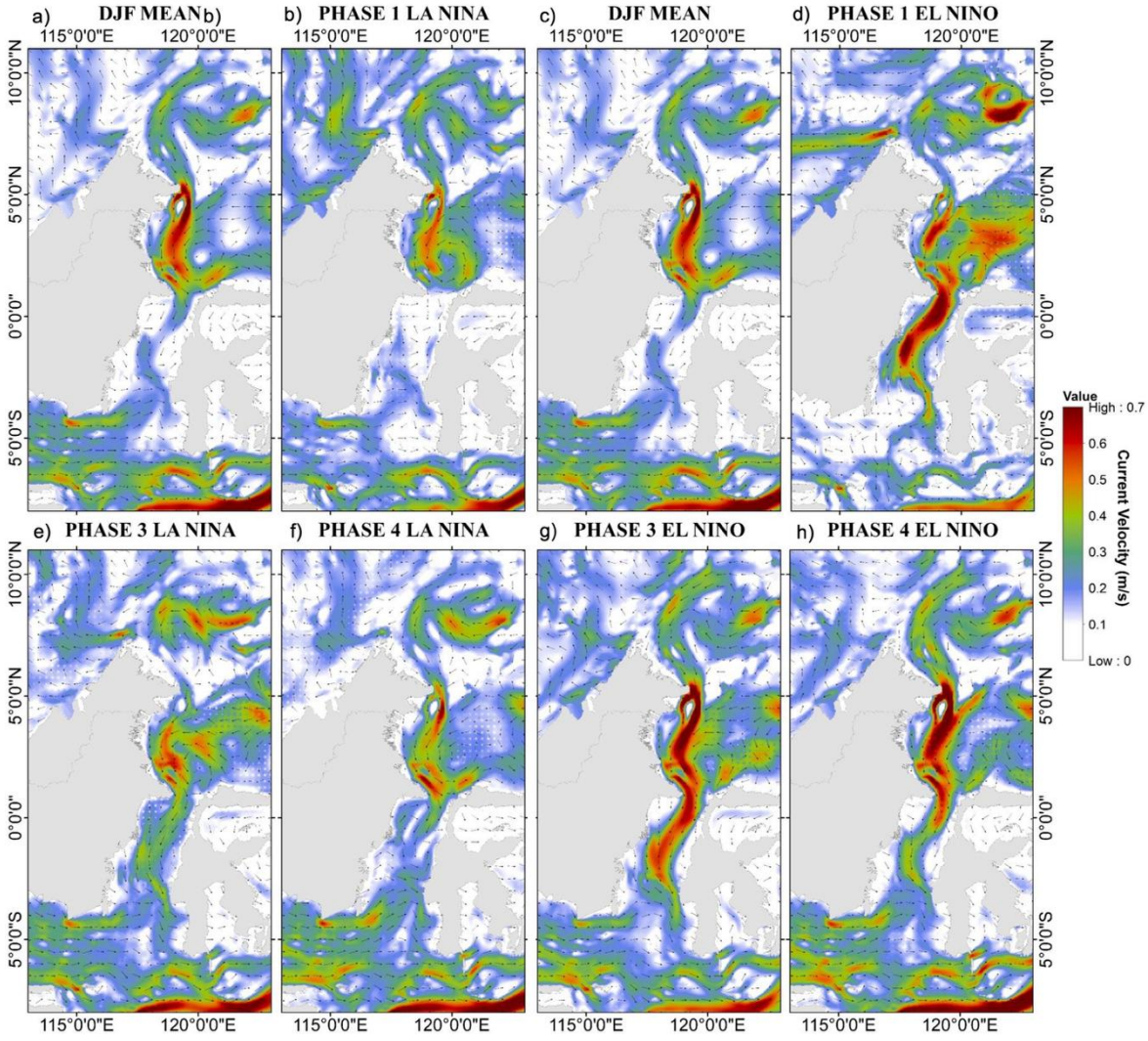
Previous studies have shown that the response of Indonesian monsoon rainfall to the MJO can be stronger during El Niño than during La Niña (Ghelani et al., 2017), while unusually strong MJO events have also been observed during El Niño conditions (Marshall et al., 2016). ENSO can influence MJO propagation, and its effects can depend on the type of El Niño (Chen et al., 2016; Pang et al., 2016). Chen et al. (2016) reported that the MJO tends to weaken during eastern Pacific El Niño events, resulting in a shorter eastward propagation range, while Li et al. (2023) found reduced MJO zonal wind amplitude during the mature stage of El Niño. These interactions may modify the influence of strong MJO events on Indonesian waters by altering the associated pressure gradient response.

In contrast, La Niña conditions are generally associated with stronger and faster MJO activity. Wei and Ren (2022) found that La Niña is associated with enhanced atmospheric moisture over the Indian Ocean and Maritime Continent, which supports stronger and faster MJO convection. In our results, however, the combination of strong MJO and La Niña produces weaker currents than strong MJO events alone. Despite this, current velocity remains higher than the climatological mean, particularly during phases 3-4, consistent with the generally stronger Makassar Throughflow during La Niña years. Previous studies also reported that

Makassar Strait transport tends to increase during La Niña and decrease during El Niño (Susanto and Song, 2015). These results indicate that the current response to the MJO depends not only on its phase but also on the background ENSO condition.

Table 3. Current velocity (m/s) of points A and B in DJF during strong MJO, strong MJO-El Niño, and strong MJO-La Niña events compared with the 2004-2020 study-period mean.

Phase	Strong MJO Event		Strong MJO & El Niño event		Strong MJO & La Niña event	
	A	B	A	B	A	B
1	0.21	0.28	0.52	0.45	0.24	0.21
3	0.41	0.40	0.51	0.46	0.33	0.36
4	0.45	0.35	0.50	0.33	0.48	0.28
Mean	0.37	0.22	0.37	0.22	0.37	0.22



330

331 **Figure 3**. Spatial distribution of DJF surface current velocity for strong MJO composites
332 (phases 1, 3, and 4) and concurrent La Niña and El Niño conditions. The 2004-2020 DJF study-
333 period mean is given for reference.

334 *3.2.2 First transitional season (March-May/MAM)*

335 During the first transitional season (MAM), current velocity increases relative to the wet
336 season, particularly in the central Makassar Strait (Figure 4). Significant differences from the
337 climatological mean occur during MJO phases 2, 3, and 7 (Table 4). At point B, the
338 climatological current velocity is approximately 0.50 m s^{-1}, increasing to 0.60 m s^{-1} during
339 phases 2-3 and decreasing to 0.41 m s^{-1} during phase 7. The intraseasonal signal is detectable
340 to approximately 25 m depth, whereas changes between 50 and 150 m are not significant.

341 Although MAM represents a transition toward the dry season, the oceanic and atmospheric
342 conditions remain strongly influenced by the preceding wet season. Consequently, MJO

influence remains pronounced during these months. During boreal winter (November-April), MJO activity is predominantly concentrated in the Southern Hemisphere (Chen et al., 2017). Although the MJO generally propagates eastward, it can turn southward or weaken while crossing the Indonesian region (Zhou and Murtugudde, 2020). Such propagation modifies the cross-strait flow and can also alter the meridional sea surface temperature (SST) gradient along the Makassar Strait. During active MJO conditions, SST is generally lower in the southern than in the northern Makassar Strait, possibly reflecting stronger ocean-atmosphere interaction in the southern region (Shinoda et al., 2016). Napitu et al. (2015) similarly showed that wet season surface heat flux contributes to SST cooling over Indonesian waters, particularly in the Southern Hemisphere.

The ITF generally strengthens during the early suppressed MJO phases (phases 1-3). Napitu et al. (2019) showed that the suppressed phase is associated with anomalous westward and southward winds over the Java Sea and Makassar Strait. These wind anomalies can lower sea level in the southern Makassar Strait through Ekman transport, thereby increasing the pressure gradient and enhancing southward ITF transport. During the active phase, in contrast, eastward wind anomalies promote accumulation of surface water in the southern Makassar Strait and reduce the pressure gradient. Intraseasonal changes in the Makassar Strait may also be connected with coastal Kelvin waves propagating from the Indian Ocean in association with the MJO (Drushka et al., 2010; Schiller et al., 2010; Zhou and Murtugudde, 2010).

The background ENSO and IOD states further modify this response. During strong MJO - El Niño events, current velocity increases substantially during phases 2-3, reaching approximately 0.80 m s^{-1}, while decreasing to approximately 0.20 m s^{-1} during phase 7 relative to the central strait climatological mean of 0.50 m s^{-1}. Under strong MJO-La Niña conditions, current velocity is weaker than during strong MJO events alone, particularly during phase 7, when it is approximately 0.40 m s^{-1}. The spatial current distribution during MJO-El Niño and MJO-positive IOD conditions is broadly similar, although the positive IOD combination produces stronger current velocities, reaching approximately 0.86 m s^{-1} during phases 2-3.

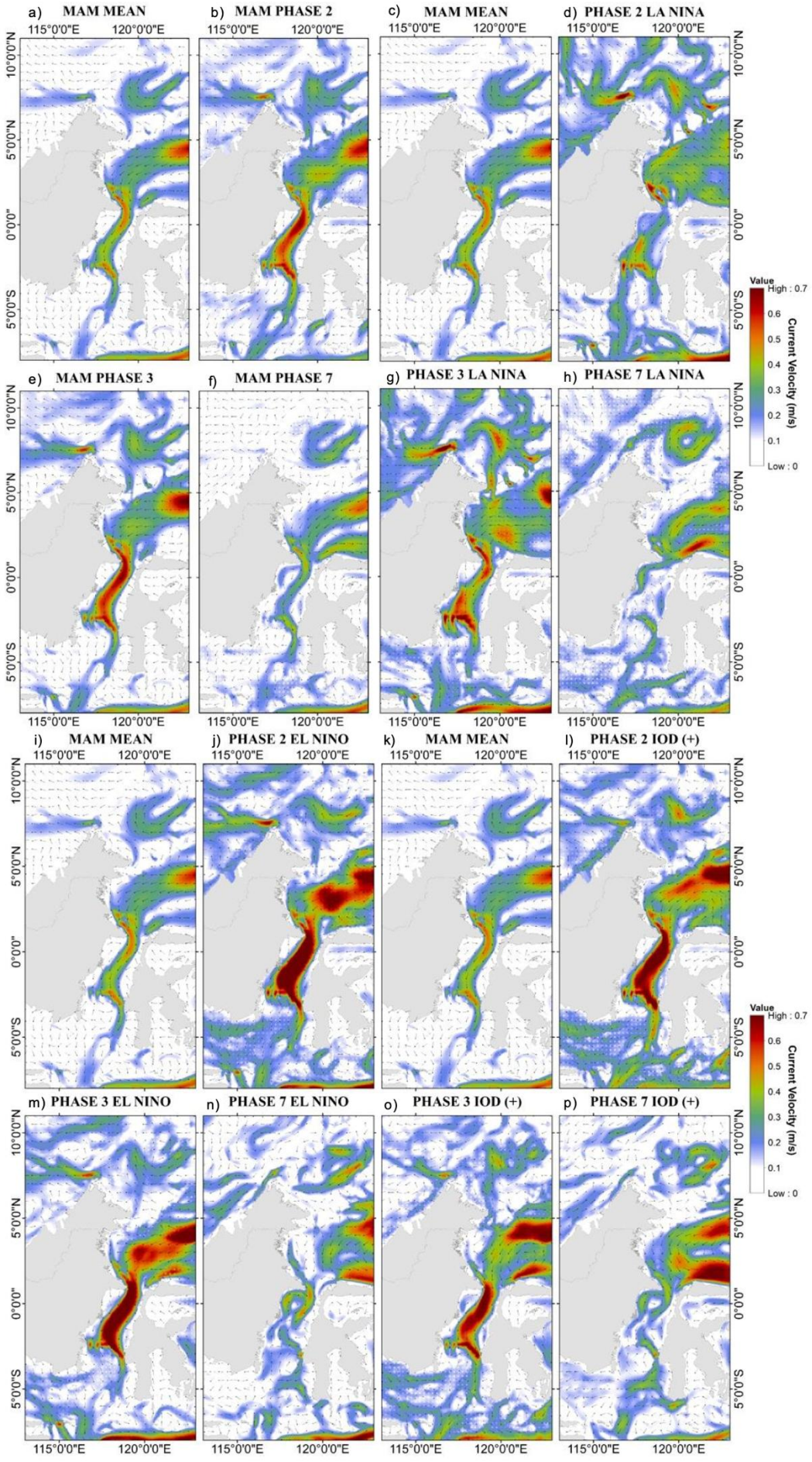
Table 4. Current velocity (m s^{-1}) at points A and B in MAM during strong MJO, strong MJO-El Niño, strong MJO-La Niña, and strong MJO-positive IOD events compared with the 2004-2020 study-period mean.

Phase	Strong MJO Event		Strong MJO & El Niño event		Strong MJO & La Niña event		Strong MJO & IOD (+) Event	
	A	B	A	B	A	B	A	B
2	0.28	0.60	0.45	0.80	0.09	0.38	0.39	0.86
3	0.39	0.59	0.48	0.69	0.25	0.56	0.40	0.70
7	0.24	0.41	0.16	0.20	0.34	0.39	0.28	0.32
Mean	0.31	0.50	0.31	0.50	0.31	0.50	0.31	0.50

374

375

376


a) MAM MEAN
b) MAM PHASE 2
c) MAM MEAN
d) PHASE 2 LA NINA
e) MAM PHASE 3
f) MAM PHASE 7
g) PHASE 3 LA NINA
h) PHASE 7 LA NINA
i) MAM MEAN
j) PHASE 2 EL NINO
k) MAM MEAN
l) PHASE 2 IOD (+)
m) PHASE 3 EL NINO
n) PHASE 7 EL NINO
o) PHASE 3 IOD (+)
p) PHASE 7 IOD (+)
115°0'0"E
120°0'0"E
10°0'0"N
5°0'0"N
0°0'0"
5°0'0"S
Value
High : 0.7
0.6
0.5
0.4
0.3
0.2
0.1
Low : 0
Current Velocity (m/s)

377

Figure 4. Spatial distribution of MAM surface current velocity for strong MJO composites (phases 2, 3, and 7) and concurrent La Niña, El Niño, and positive IOD conditions. The 2004-2020 MAM study-period mean is given for reference.

3.2.3 Dry season (June-August/JJA)

During the dry season (JJA), the Makassar Throughflow exhibits strong southward transport, consistent with previous observations and modeling studies (Gordon et al., 2008). Significant intraseasonal variability in current velocity during strong MJO events occurs in phases 2, 3, 6, and 7 (Figure 5). The current becomes particularly prominent in the southern Makassar Strait near the Labani channel and Dewakang sill. Current velocity increases during phases 2-3 relative to the climatological mean as the MJO approaches Indonesia (Table 5). At point A, current velocity increases to approximately 0.43-0.54 m s^{-1}, with the increase extending across much of the strait. Nevertheless, surface current variability associated with the MJO is generally weaker during JJA than during the wet season, consistent with the weaker intraseasonal OLR variability reported by Napitu et al. (2015, 2019).

During phases 6-7, current velocity at point A decreases to approximately 0.12-0.28 m s^{-1}. At point B, however, the current strengthens during the dry season phases, increasing from the climatological value of approximately 0.50 m s^{-1} to nearly 0.99 m s^{-1}. The relatively low correlation between current velocity and the MJO index during JJA indicates that seasonal monsoonal forcing is more important than the MJO in determining the overall current state during this season. During the northwest monsoon, low-salinity surface water from the Java Sea moves southward into the Makassar Strait, whereas during the southeast monsoon, southeasterly winds return low-salinity water toward the Java Sea (Gordon et al., 2003). These winds also transport Makassar Strait water toward the Java Sea, thereby increasing transport through the Makassar Strait and reducing South China Sea throughflow through the Karimata Strait (Susanto et al., 2012).

Although the MJO influence is weaker during the dry season than during the wet season, significant phase-dependent changes remain evident. The MJO-La Niña current distribution is generally similar to that during strong MJO events alone. In contrast, the MJO-El Niño current is weaker than the strong MJO response, although it remains stronger than the climatological mean during phases 2-3, reaching approximately 0.72 m s^{-1} at point B. During phases 6-7, the current decreases to approximately 0.57 m s^{-1}. Positive IOD conditions produce significant

changes relative to MJO only events, particularly a weakening during phase 2 and strengthening during phase 7.

Table 5. Current velocity (m s^{-1}) at points A and B in JJA during strong MJO, strong MJO - El Niño, strong MJO-La Niña, and strong MJO-positive IOD events compared with the 2004-2020 study-period mean.

Phase	Strong MJO Event		Strong MJO & El Niño event		Strong MJO & La Niña event		Strong MJO & IOD (+) Event	
	A	B	A	B	A	B	A	B
2	0.43	0.93	0.35	0.93	0.43	0.99	0.45	0.81
3	0.54	0.99	0.53	0.72	0.48	1.06	0.60	1.04
6	0.28	0.71	0.49	0.63	0.62	0.71	0.20	0.70
7	0.12	0.68	0.23	0.57	0.27	0.66	0.50	1.09
Mean	0.31	0.50	0.31	0.50	0.31	0.50	0.31	0.50

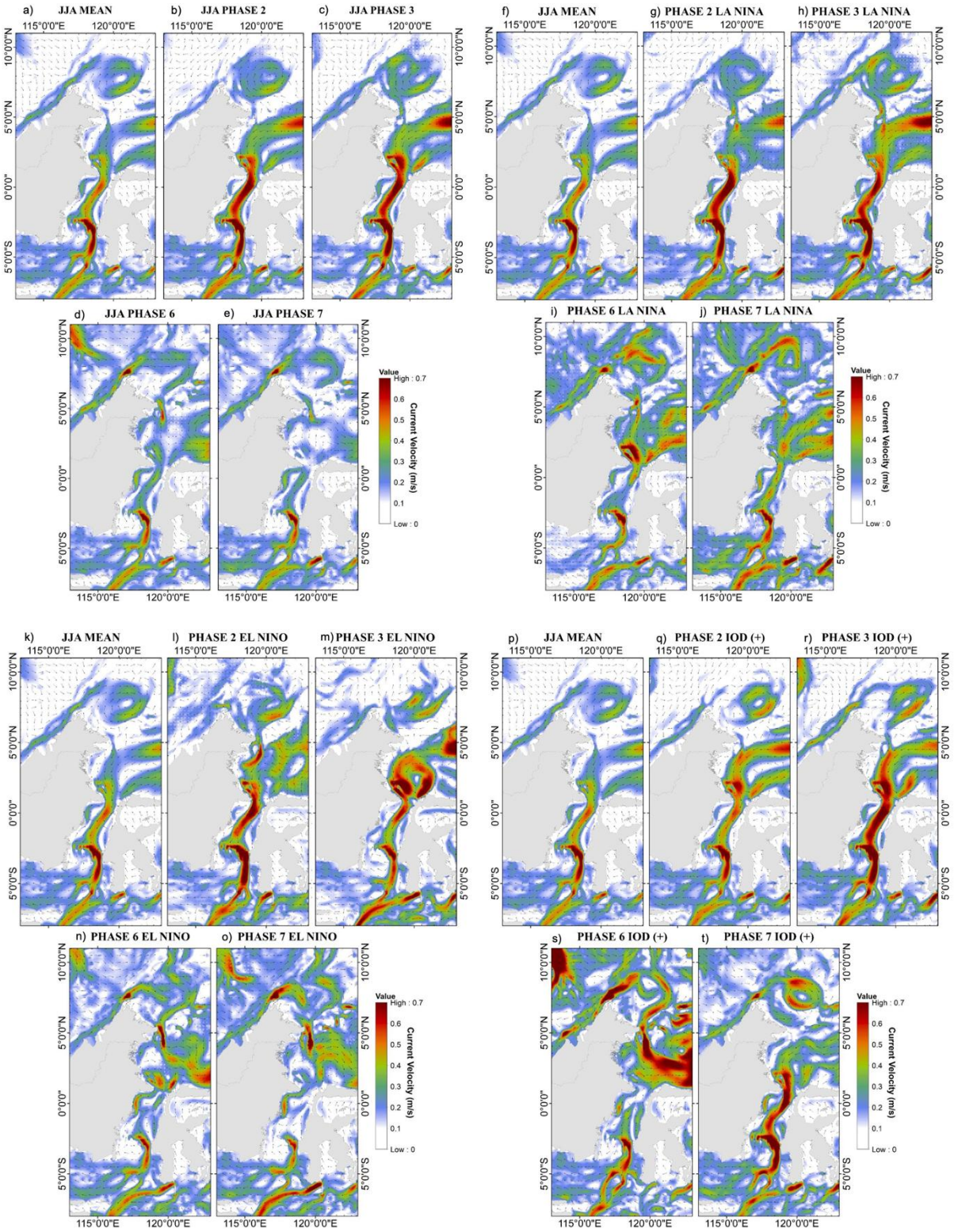


Figure 5. Spatial distribution of JJA surface current velocity for strong MJO composites (phases 2, 3, 6, and 7) and concurrent La Niña, El Niño, and positive IOD conditions. The 2004-2020 JJA study-period mean is given for reference.

3.2.4 Second transitional season (September-November/SON)

During the second transitional season (SON), significant intraseasonal variability is evident throughout the Makassar Strait (Figure 6). In contrast to the wet season, surface current velocities are relatively strong. Current velocity tends to increase during phases 1-2, with point B increasing from a climatological mean of 0.81 m s^{-1} to approximately 0.90 m s^{-1} (Table 6). During phases 6-7, however, current velocity at point B decreases to approximately 0.50 m s^{-1}. The weakening during phase 7 extends to approximately 50 m depth, where the current decreases from a climatological mean of 0.83 m s^{-1} to 0.59 m s^{-1}.

Regional geography and bathymetry may contribute to the observed current structure. Currents during SON remain strong, similar to JJA, in the central Makassar Strait before turning southward as they pass through the Dewakang Sill. The sill has a depth of approximately 680 m and constrains the flow through the strait. The narrowing of the flow pathway can increase current velocity through the channel and may enhance mixing and turbulence around the sill (Gordon et al., 2019).

Internal tides provide another mechanism that may influence the vertical structure and variability of Makassar Strait currents. At the Dewakang Sill, internal tidal variability arises from vertical differences in temperature, salinity, and density, generating depth-dependent flows. These internal tides are among the processes influencing ocean dynamics and deep water mixing in the Labani channel (Horhoruw et al., 2015). Therefore, it is important to note that the observed intraseasonal current response during SON may reflect the combined influence of atmospheric forcing, regional circulation, bathymetric constraints, and internal ocean dynamics.

During MJO-La Niña events, no significant phase-dependent changes are observed relative to strong MJO events alone, similar to the response during the preceding season. In contrast, MJO-El Niño conditions produce a marked reduction in current velocity in the central strait during phases 6-7, decreasing to approximately 0.40 m s^{-1} compared with the climatological mean of 0.81 m s^{-1}. The MJO-positive IOD combination generally strengthens the current relative to strong MJO events alone. Positive IOD events are associated with reduced SST and rainfall over Indonesia (Nurdiati et al., 2022), and the IOD typically reaches its maximum amplitude during SON, when positive IOD years are associated with negative rainfall anomalies over Indonesia (Ratna et al., 2017). The influence of ENSO and IOD on Indonesian

rainfall develops from JJA and extends into the DJF period (As-syakur et al., 2014), providing an important seasonal background for interpreting the SON current response.

Table 6. Current velocity (m s^{-1}) at points A and B in SON during strong MJO, strong MJO-El Niño, strong MJO-La Niña, and strong MJO-positive IOD events compared with the 2004-2020 study-period mean.

Phase	Strong MJO Event		Strong MJO & El Niño event		Strong MJO & La Niña event		Strong MJO & IOD (+) Event	
	A	B	A	B	A	B	A	B
1	0.71	0.91	0.70	0.86	0.68	0.80	0.66	1.05
2	0.64	0.88	0.61	0.84	0.64	0.92	0.70	0.96
6	0.54	0.59	0.71	0.40	0.46	0.49	0.81	0.89
7	0.61	0.46	0.80	0.42	0.54	0.38	0.93	0.78
Mean	0.62	0.81	0.62	0.81	0.62	0.81	0.62	0.81

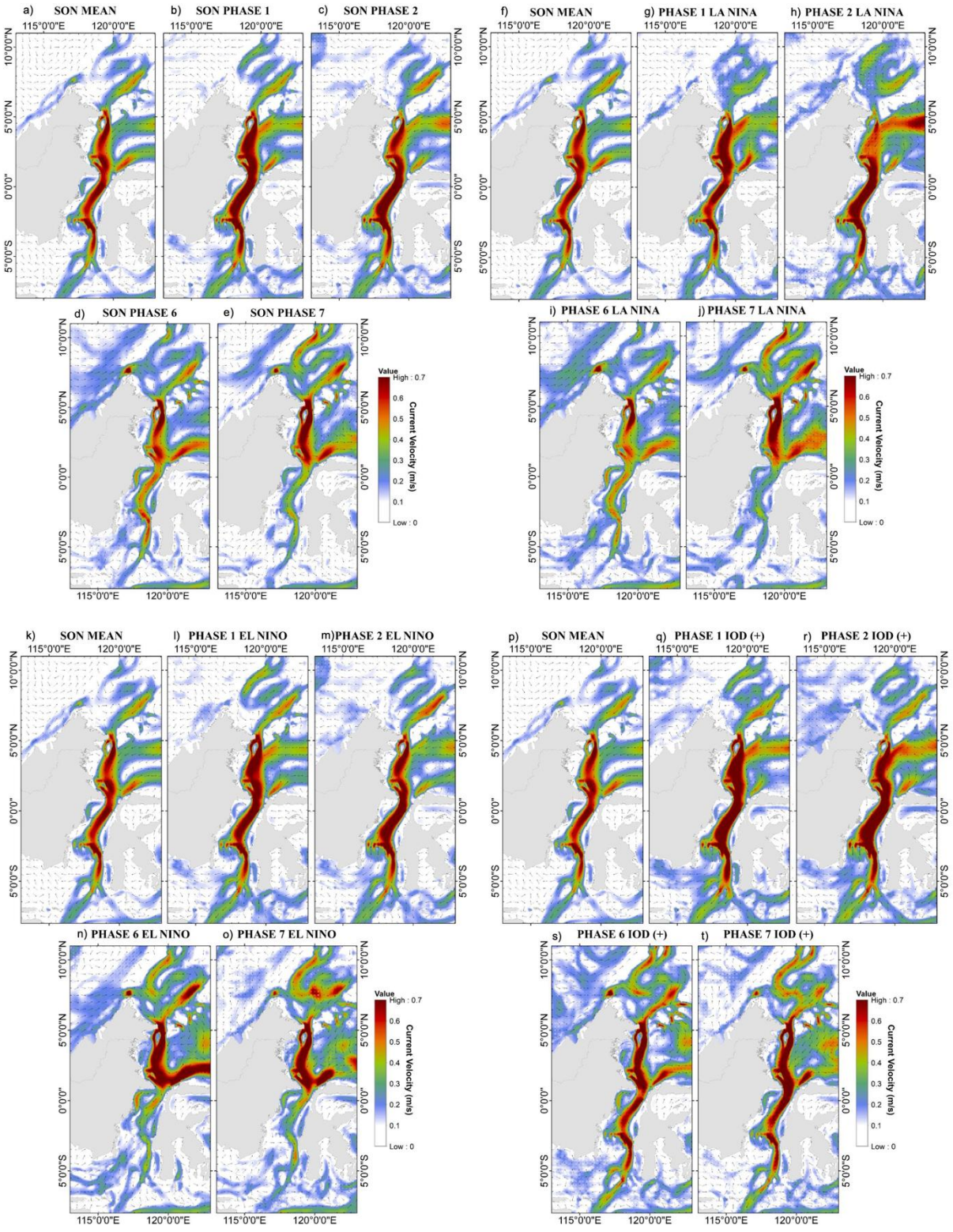


Figure 6. Spatial distribution of SON surface current velocity for strong MJO composites (phases 1, 2, 6, and 7) and concurrent La Niña, El Niño, and positive IOD conditions. The 2004-2020 SON study-period mean is given for reference.

3.3 Volume Transport and Vertical Structure

Current velocity describes the local intensity and direction of flow, whereas volume transport represents the integrated amount of water crossing a specified cross-sectional area per unit time. To quantify the transport response associated with strong MJO events and its modulation by ENSO and IOD, volume transport was calculated at two selected locations over the 17-year study period (Figure 1) and evaluated by season and MJO phase. Point B, located in the central Makassar Strait near the INSTANT observation site in the Labani channel at the Dewakang Sill, is mainly relevant to the main Makassar Strait ITF pathway. The Dewakang Sill is an important control point for water mass transformation, turbulent mixing, and regional circulation. The vertical distribution of transport shows the largest southward transport near 100 m depth. This is consistent with the thermocline centered vertical structure reported by Gordon et al. (2012).

Although volume transport was calculated at both points A and B, the depth-resolved composite profiles shown in Figures 7 and 8 focus on point B, where the main Makassar Strait ITF pathway and the INSTANT observation site are located. At point B, depth-resolved transport generally shows limited phase-to-phase variability from the wet season (DJF) through the first transitional season (MAM) (Figure 7). For the layer represented by the 100-m depth level, the southward transport magnitude ranges from approximately 1.1 to 2.7 Sv, with the highest values occurring during MJO phase 7 in DJF and phase 8 in MAM.

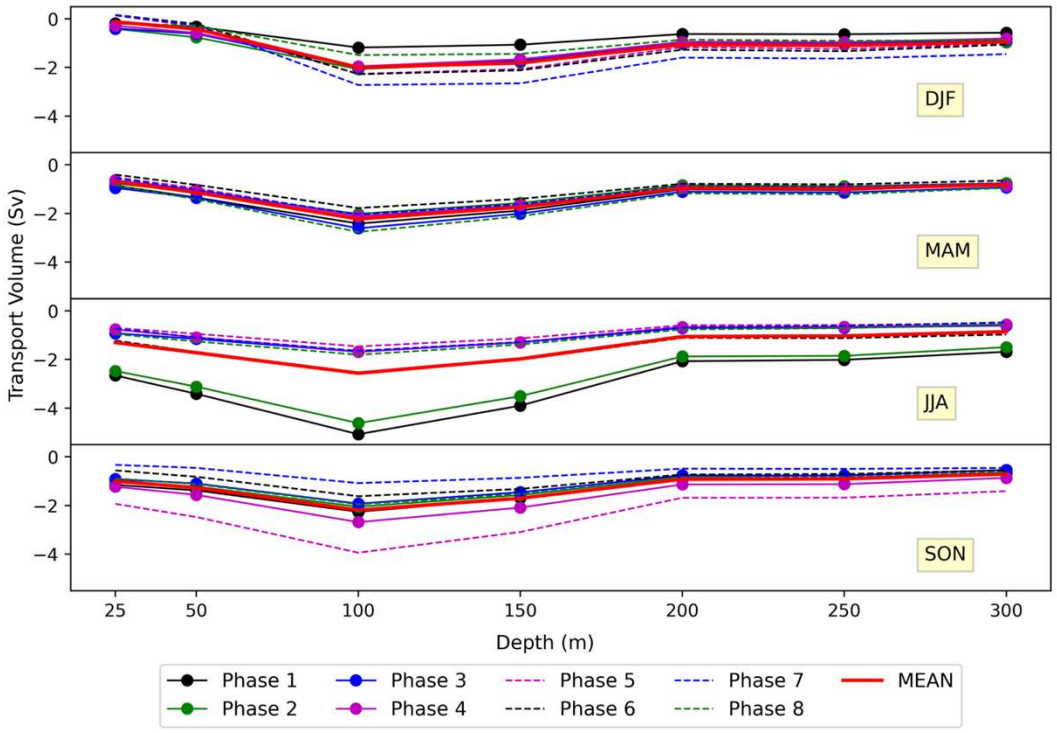


Figure 7. MJO-phase and seasonal volume transport at point B, around the Labani channel near the INSTANT mooring site, under strong MJO conditions.

A pronounced intraseasonal response in depth-resolved volume transport occurs during the dry season (JJA). This period coincides with the Northern Hemisphere Summer Monsoon (NHSM), when the Makassar Throughflow is characterized by stronger southward transport than during boreal winter (Gordon et al., 2019). Changes in atmospheric circulation associated with the Asian and Australia-Indonesia monsoons can strengthen easterly winds over the western Pacific (Wang and Xie, 1997). Consistent with this seasonal forcing, the southward transport magnitude for the layer represented by the 100-m depth level increases markedly during MJO phases 1-2, reaching approximately 4.7-5.0 Sv, compared with approximately 1.6 Sv during the other phases.

ENSO further modulates the MJO-related transport response. Previous studies indicate that La Niña generally enhances Makassar Strait transport, whereas El Niño reduces it (Gordon et al., 2019). In the present analysis, however, the combination of La Niña and strong MJO conditions produces a lower southward transport magnitude than strong MJO conditions alone, particularly during phases 1-3, when it decreases to approximately 3.4 Sv. Under MJO-El Niño conditions, the southward transport magnitude during phase 2 decreases to approximately 2.2 Sv. This reduction is consistent with the previously documented association between MJO

activity and weakening of surface-layer ITF transport in the Makassar Strait during boreal summer (Napitu et al., 2019).

The combination of strong MJO and positive IOD produces a distinct phase-dependent transport response during JJA. The southward transport magnitude remains relatively high during phases 1-4, at approximately 2-4 Sv, but decreases substantially during phases 5-8 to approximately 0.4-0.9 Sv. This phase-dependent response suggests that positive IOD conditions modify the MJO-related transport signal predominantly during the latter MJO phases, resulting in an overall reduction in transport during phases 5-8 (Figure 8).

During the second transitional season (SON), the southward transport magnitude increases during phase 5, when the MJO convective center is located over Indonesia, reaching a maximum of approximately 3.9 Sv. Variability in volume transport may also be influenced by geostrophic wind forcing and Kelvin waves associated with MJO activity in the Indian Ocean and along the southern coast of Java (Chong et al., 2000). One possible mechanism for reduced transport during the transitional seasons is the propagation of Kelvin waves trapped along the Sumatra coast, which can extend toward southern Java and subsequently influence the Makassar Strait (Syamsudin et al., 2004; Pujiana et al., 2019).

The interaction between MJO and El Niño during SON is associated with enhanced southward transport magnitude, with a maximum of approximately 3.4 Sv during phase 4. Under positive IOD conditions, the most pronounced changes occur during phases 8 and 1, when the southward transport magnitude reaches approximately 4 Sv. Taken together, these results demonstrate that the intraseasonal volume-transport response in the Makassar Strait is strongly season-dependent. The response reflects the combined influence of MJO phase and background monsoonal forcing, with ENSO and IOD providing additional modulation and remotely forced oceanic signals, including Kelvin waves, potentially contributing to transport variability during the transitional seasons.

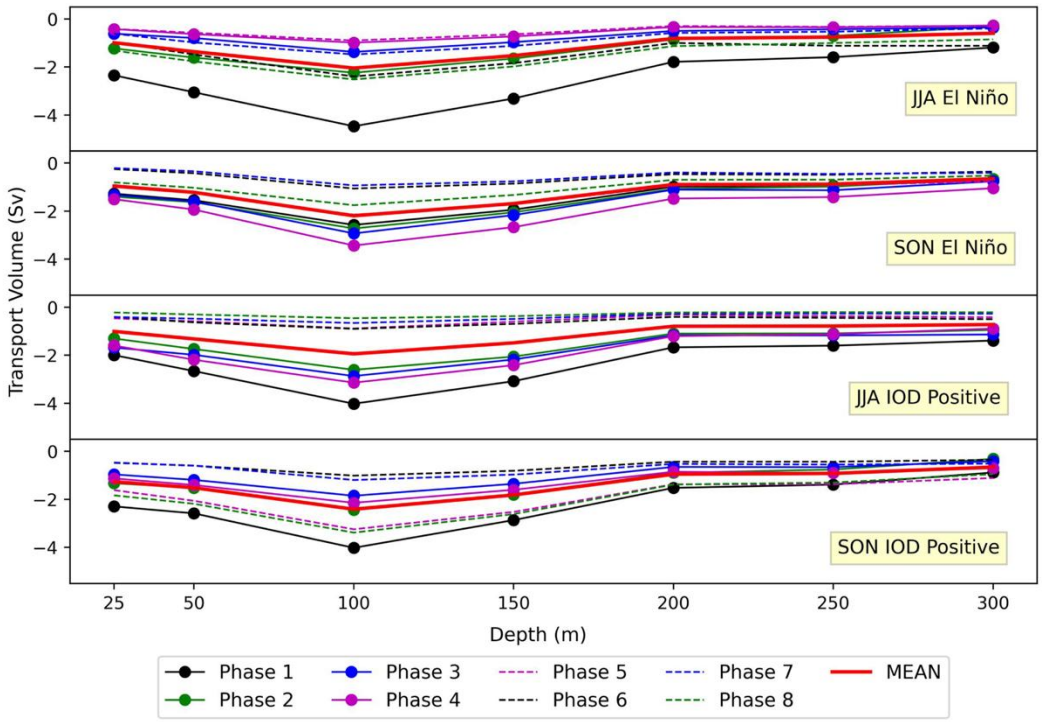


Figure 8. MJO-phase dependence of depth-resolved volume transport at point B near the Labani Channel and the INSTANT mooring site under concurrent strong MJO-El Niño and strong MJO-positive IOD conditions.

4. Discussion

4.1 Seasonal Background and MJO Phase Dependence

The results support a schematic view of Makassar Strait variability in which the monsoon establishes the seasonal circulation condition and the MJO modulates it on intraseasonal timescales. The contrast between DJF and JJA is important in the way that surface current variability associated with the MJO is relatively prominent during the wet season, whereas the largest volume transport response occurs during the dry season. However, the same MJO phase cannot be interpreted independently of the seasonal background.

The phase dependence is physically consistent with changes in the along-strait pressure gradient. During suppressed MJO phases, anomalous westward and southward winds can drive Ekman transport and lower sea level in the southern Makassar Strait, strengthening the pressure gradient that supports southward ITF flow. During active phases, eastward wind anomalies can promote surface water accumulation and weaken that gradient (Napitu et al., 2019). Coastally trapped Kelvin waves associated with MJO forcing may provide an additional pathway linking

Indian Ocean disturbances to Makassar Strait variability (Drushka et al., 2010; Schiller et al., 2010; Zhou and Murtugudde, 2010).

The seasonal contrast therefore does not imply a weaker role for the MJO in JJA. Instead, strong monsoonal forcing dominates the surface current field while the MJO signal can emerge more clearly in the integrated thermocline transport.

4.2 Vertical Structure: Surface Current versus ITF Transport

A central implication is that surface current velocity and ITF volume transport should not be treated as interchangeable measures. The largest southward transport occurs near 70-120 m within the thermocline, and the strongest composite response reaches approximately 4.7-5.0 Sv at 100 m during JJA phases 1-2. This vertical structure is consistent with the established thermocline pathway of the Makassar Strait ITF (Gordon et al., 2012).

The different behavior of surface velocity and transport helps explain why JJA can exhibit a relatively weak correlation between surface current velocity and the MJO index while exhibiting a strong transport response. MJO-related wind forcing can modify sea level gradients and upper-ocean circulation without producing a proportional surface current anomaly.

The validation results constrain this interpretation. GLORYS12 reproduces variability reasonably well in the upper and intermediate layers, with the strongest monotonic agreement at 350 m, whereas the 750 m correlation is weak and negative. The inferred MJO-related vertical structure should therefore be interpreted cautiously in the deepest layer.

4.3 State-Dependent ENSO and IOD Modulation

The combined composites demonstrate that ENSO does not simply amplify or suppress the MJO response uniformly. El Niño enhances selected early-phase surface currents during DJF and MAM but is associated with reduced transport during selected later phases in JJA and SON. This contrast is consistent with a background state interpretation in which ENSO modifies the basin-scale pressure gradient and thermocline environment in which the intraseasonal wind forcing acts. The response is therefore not adequately described as a simple linear sum of MJO and ENSO effects.

La Niña provides a complementary result. Although the mean Makassar Strait Throughflow is generally stronger during La Niña, the strong MJO composites do not show a proportional

increase in the MJO anomaly. In several cases, the combined MJO-La Niña response is weaker than the MJO only response. Therefore, the amplitude of an intraseasonal perturbation depends on the background circulation rather than simply scaling with the mean transport.

Positive IOD conditions introduce another seasonal asymmetry, most clearly during JJA-SON. The JJA transport response is reduced during later MJO phases, whereas the SON surface current response is enhanced during selected phases. Because the IOD is strongest during SON, Indian Ocean boundary forcing may alter the expression of MJO variability within the Makassar Strait.

4.4 Implications and Limitations

The results indicate that Makassar Strait ITF variability should be interpreted as a multiscale interaction rather than as the response to an isolated climate mode. The monsoon determines the seasonal state, ENSO and IOD modify the interannual background, and the MJO perturbs that state on intraseasonal timescales. This framework helps explain why the same MJO phase can produce different current and transport responses in different seasons or ENSO/IOD states. Because the ITF redistributes heat between the Pacific and Indian Oceans, transport changes of several Sverdrups may be relevant to short-term interbasin heat exchange.

Several limitations should be recognized. The analysis focuses on strong MJO events and does not represent all intraseasonal variability. The ENSO and IOD composites contain fewer daily sample sizes than the MJO-only composites, and some phase-specific composites are based on relatively few samples, their differences should be interpreted as state-dependent patterns rather than universal responses. The weak validation correlation at 750 m also limits interpretation of MJO-related variability in the deepest layer. Additional long-term mooring observations and lagged wind-transport analyses would help test the proposed pressure-gradient mechanism. A more detailed investigation of the subsurface transport maximum, following approaches such as Nie et al. (2026), is left for a subsequent study.

5. Conclusions

This study examined seasonal and intraseasonal variability of the Makassar Strait Indonesian Throughflow (ITF) during strong MJO events and assessed how the response varies under concurrent ENSO and IOD conditions. The analysis used daily GLORYS12 reanalysis data for 2004-2020, evaluated against INSTANT mooring observations.

First, Makassar Strait circulation exhibits clear MJO phase dependence, with early suppressed phases generally favoring stronger southward flow and later active phases associated with weaker or deflected surface currents. The magnitude of this response varies strongly among seasons.

Second, the ITF response is vertically structured. The largest southward transport occurs within the thermocline, around 70-120 m, and reaches approximately 4.7-5.0 Sv for the layer represented by the 100-m nominal depth during JJA phases 1-2. Surface current anomalies do not fully characterize intraseasonal ITF transport variability.

Third, ENSO and IOD modify the MJO response according to the background state and season. El Niño enhances selected early-phase surface-current responses but is associated with reduced transport during selected later phases. La Niña does not proportionally amplify the MJO-related anomaly despite the generally stronger background throughflow. Positive IOD conditions introduce additional phase- and season-dependent modulation, eventually during JJA and SON.

Overall, the Makassar Strait acts as a dynamically sensitive gateway in which seasonal monsoon forcing, basin-scale climate variability, and intraseasonal MJO forcing interact. The results emphasize that MJO-related ITF variability should be evaluated together with the background oceanic state and its vertical structure.

Acknowledgments.

The authors acknowledge the International Nusantara Stratification and Transport (INSTANT) program for the mooring observations used in this study, and especially the Lamont-Doherty Earth Observatory (LDEO), Columbia University, for providing and processing the Makassar Strait mooring data. The authors also acknowledge the Copernicus Marine Service for providing the GLORYS12 ocean reanalysis data. This study was supported by the International Exchange Program of the National Institute of Information and Communications Technology (NICT) during the first author's visit to the Graduate School of Advanced Science and Engineering, Hiroshima University, in fiscal year 2026/2027.

640 REFERENCES

641

642 Amaya DJ, Alexander MA, Scott JD, Jacox MG (2023) An evaluation of high-resolution ocean
643 reanalyses in the California Current System. Prog Oceanogr 210:102951.
644 https://doi.org/10.1016/j.pocean.2022.102951

645 As-syakur AR, Adnyana IWS, Mahendra MS et al (2014) Observation of spatial patterns on
646 the rainfall response to ENSO and IOD over Indonesia using TRMM Multisatellite
647 Precipitation Analysis (TMPA). Int J Climatol 34(15):3825-3839.
648 https://doi.org/10.1002/joc.3939

649 Birch CE, Webster S, Peatman SC et al (2016) Scale interactions between the MJO and the
650 western Maritime Continent. J Climate 29(7):2471-2492. https://doi.org/10.1175/JCLI-D-
651 15-0557.1

652 Chen X, Li C, Tan Y (2017) Further inquiry into characteristics of MJO in boreal winter. Int J
653 Climatol 37(12):4451-4462. https://doi.org/10.1002/joc.5098

654 Chen X, Ling J, Li C (2016) Evolution of the Madden-Julian oscillation in two types of El
655 Niño. J Climate 29(5):1919-1934. https://doi.org/10.1175/JCLI-D-15-0486.1

656 Chong JC, Sprintall J, Hautala S et al (2000) Shallow throughflow variability in the outflow
657 straits of Indonesia. Geophys Res Lett 27(1):125-128.
658 https://doi.org/10.1029/1999GL002338

659 Cleveland RB, Cleveland WS, McRae JE et al (1990) STL: a seasonal-trend decomposition
660 procedure based on loess. J Off Stat 6:3-73

661 Drushka K, Sprintall J, Gille ST, Brodjonegoro I (2010) Vertical structure of Kelvin waves in
662 the Indonesian throughflow exit passages. J Phys Oceanogr 40(9):1965-1987.
663 https://doi.org/10.1175/2010JPO4380.1

664 Ghelani RPS, Oliver ECJ, Holbrook NJ et al (2017) Joint modulation of intraseasonal rainfall
665 in tropical Australia by the Madden-Julian Oscillation and El Niño-Southern Oscillation.
666 Geophys Res Lett 44(20):10754-10761. https://doi.org/10.1002/2017GL075452

667 Gordon AL (1986) Interocean exchange of thermocline water. J Geophys Res 91(C4):5037-
668 5046. https://doi.org/10.1029/JC091iC04p05037

669 Gordon AL (2005) Oceanography of the Indonesian seas and their throughflow. Oceanography
670 18(4):15-27. https://doi.org/10.5670/oceanog.2005.01

671 Gordon AL, Napitu A, Huber BA et al (2019) Makassar Strait throughflow seasonal and
672 interannual variability: an overview. J Geophys Res Oceans 124(6):3724-3736.
673 https://doi.org/10.1029/2018JC014502

674 Gordon AL, Huber BA, Metzger EJ, Susanto RD, Hurlburt HE, Adi TR (2012) South China
675 Sea throughflow impact on the Indonesian throughflow. Geophys Res Lett 39:L11602.
676 https://doi.org/10.1029/2012GL052021

677 Gordon AL, Susanto RD, Ffield A et al (2008) Makassar Strait throughflow, 2004 to 2006.
678 Geophys Res Lett 35:L24605. https://doi.org/10.1029/2008GL036372

679 Gordon AL, Susanto RD, Vranes K (2003) Cool Indonesian throughflow as a consequence of
680 restricted surface layer flow. Nature 425:824-828. https://doi.org/10.1038/nature02038

681 Horhoruw SM, Atmadipoera AS, Purba M, Purwandana A (2015) Current structure and spatial
682 variation of Indonesian Throughflow in Makassar Strait under EWIN 2013. Ilmu Kelautan
683 20(2):87-100. https://doi.org/10.14710/ik.ijms.20.2.87-100

684 Jean-Michel L, Greiner E, Bourdallé-Badie R et al (2021) The Copernicus Global 1/12°
685 Oceanic and Sea Ice GLORYS12 Reanalysis. Front Earth Sci 9:698876.
686 https://doi.org/10.3389/feart.2021.698876

687 Lestari S, King A, Vincent C et al (2022) Variability of Jakarta rain-rate characteristics
688 associated with the Madden-Julian Oscillation and topography. Mon Weather Rev
689 150(8):1953-1975. https://doi.org/10.1175/MWR-D-21-0112.1

690 Lestari, S., N. Takahashi, F. Syamsudin, C. Vincent, and S. Mori (2026) Statistical properties
691 of stratiform and convective rain rates under seasonal changes and MJO propagation at
692 Jakarta, the Maritime Continent. Mon. Wea. Rev., 154, 445-
693 468, https://doi.org/10.1175/MWR-D-25-0105.1.

694 Li L, Chen X, Li C et al (2023) Comparison of Madden-Julian oscillation in three super El
695 Niño events. Front Earth Sci 10:1021953. https://doi.org/10.3389/feart.2022.1021953

696 Madden RA, Julian PR (1971) Detection of a 40-50 day oscillation in the zonal wind in the
697 tropical Pacific. J Atmos Sci 28:702-708

698 Madden RA, Julian PR (1972) Description of global-scale circulation cells in the tropics with
699 a 40–50 day period. J Atmos Sci 29(6):1109-1123. https://doi.org/10.1175/1520-
700 0469(1972)029<1109:DOGSCC>2.0.CO;2

701 Marshall AG, Hendon HH, Wang G (2016) On the role of anomalous ocean surface
702 temperatures for promoting the record Madden-Julian Oscillation in March 2015. Geophys
703 Res Lett 43(1):472-481. https://doi.org/10.1002/2015GL066984

704 McPhaden MJ, Santoso A, Cai W (eds) (2021) El Niño Southern Oscillation in a changing
705 climate. Geophys Monogr Ser. Wiley/AGU, Washington, DC.
706 https://doi.org/10.1002/9781119548164

707 Nagura M, McPhaden MJ (2010) Dynamics of zonal current variations associated with the
708 Indian Ocean Dipole. J Geophys Res Oceans 115:C11026.
709 https://doi.org/10.1029/2010JC006423

710 Napitu AM, Gordon AL, Pujiana K (2015) Intraseasonal sea surface temperature variability
711 across the Indonesian seas. J Climate 28(22):8710-8727. https://doi.org/10.1175/JCLI-D-14-
712 00758.1

713 Napitu AM, Pujiana K, Gordon AL (2019) The Madden-Julian Oscillation's impact on the
714 Makassar Strait surface layer transport. J Geophys Res Oceans 124:3538-3550.
715 https://doi.org/10.1029/2018JC014729

716 Nie Y, Li M, Jiang G, Hu S, Gordon AL, Li J, Wei J, Wang D (2026) The role of wind in
717 driving the subsurface velocity maxima of Makassar Strait Throughflow and Mindanao
718 Current. J Phys Oceanogr 56(6):1281-1298. https://doi.org/10.1175/JPO-D-25-0160.1

719 Nurdiati S, Najib MK, Thalib AS (2022) Joint distribution and coincidence probability of the
720 number of dry days and the total amount of precipitation in southern Sumatra fire-prone area.
721 Geographia Technica 17(2):107-118. https://doi.org/10.21163/GT_2022.172.10

722 Pang B, Chen Z, Wen Z, Lu R (2016) Impacts of two types of El Niño on the MJO during
723 boreal winter. Adv Atmos Sci 33(8):979-986. https://doi.org/10.1007/s00376-016-5272-2

724 Peatman SC, Matthews AJ, Stevens DP (2014) Propagation of the Madden-Julian Oscillation
725 through the Maritime Continent and scale interaction with the diurnal cycle of precipitation.
726 Q J R Meteorol Soc 140(680):814-825. https://doi.org/10.1002/qj.2161

727 Pei S, Shinoda T, Steffen J, Seo H (2021) Substantial sea surface temperature cooling in the
728 Banda Sea associated with the Madden-Julian Oscillation in the boreal winter of 2015. J
729 Geophys Res Oceans 126(6):e2021JC017226. https://doi.org/10.1029/2021JC017226

730 Pujiana K, McPhaden MJ, Gordon AL, Napitu AM (2019) Unprecedented response of
731 Indonesian Throughflow to anomalous Indo-Pacific climatic forcing in 2016. J Geophys Res
732 Oceans 124(6):3737-3754. https://doi.org/10.1029/2018JC014574

733 Ratna SB, Ratnam JV, Behera SK et al (2017) Validation of the WRF regional climate model
734 over the subregions of Southeast Asia: climatology and interannual variability. Clim Res
735 71(3):263-280. https://doi.org/10.3354/cr01445

736 Rauniyar SP, Walsh KJE (2011) Scale interaction of the diurnal cycle of rainfall over the
737 Maritime Continent and Australia: Influence of the MJO. J Climate 24(2):325-348.
738 https://doi.org/10.1175/2010JCLI3673.1

739 Saji NH, Yamagata T (2003) Possible impacts of Indian Ocean Dipole mode events on global
740 climate. Clim Res 25(2):151-169. https://doi.org/10.3354/cr025151

741 Schiller A, Wijffels SE, Sprintall J et al (2010) Pathways of intraseasonal variability in the
742 Indonesian Throughflow region. Dyn Atmos Oceans 50(2):174-200.
743 https://doi.org/10.1016/j.dynatmoce.2010.02.003

744 Shinoda T, Han W, Jensen TG et al (2016) Impact of the Madden-Julian Oscillation on the
745 Indonesian Throughflow in the Makassar Strait during the CINDY/DYNAMO field
746 campaign. J Climate 29(17):6085-6108. https://doi.org/10.1175/JCLI-D-15-0711.1

747 Song Q, Gordon AL (2004) Significance of the vertical profile of the Indonesian Throughflow
748 transport to the Indian Ocean. Geophys Res Lett 31:L16307.
749 https://doi.org/10.1029/2004GL020360

750 Sprintall J, Gordon AL, Koch-Larrouy A et al (2014) The Indonesian seas and their role in the
751 coupled ocean–climate system. Nat Geosci 7:487-492. https://doi.org/10.1038/ngeo2188

752 Sprintall J, Wijffels S, Gordon AL et al (2004) INSTANT: a new international array to measure
753 the Indonesian Throughflow. Eos Trans AGU 85(39):369.
754 https://doi.org/10.1029/2004EO390002

755 Susanto RD, Ffield A, Gordon AL, Adi TR (2012) Variability of Indonesian throughflow
756 within Makassar Strait, 2004-2009. J Geophys Res Oceans 117:C09033.
757 https://doi.org/10.1029/2012JC008096

758 Susanto RD, Gordon AL (2005) Velocity and transport of the Makassar Strait throughflow. J
759 Geophys Res 110:C01005. https://doi.org/10.1029/2004JC002425

760 Susanto RD, Song YT (2015) Indonesian throughflow proxy from satellite altimeters and
761 gravimeters. J Geophys Res Oceans 120(4):2844-2855.
762 https://doi.org/10.1002/2014JC010382

763 Syamsudin F, Kaneko A, Haidvogel DB (2004) Numerical and observational estimates of
764 Indian Ocean Kelvin wave intrusion into Lombok Strait. Geophys Res Lett 31:L24307.
765 https://doi.org/10.1029/2004GL021227

766 Tamasiunas MCN, Shinoda T, Susanto RD et al (2021) Intraseasonal variability of the
767 Indonesian throughflow associated with the Madden-Julian Oscillation. Deep Sea Res Part
768 II 193:104985. https://doi.org/10.1016/j.dsr2.2021.104985

769 Wang B, Xie X (1997) A model for the boreal summer intraseasonal oscillation. J Atmos Sci
770 54(1):72-86. https://doi.org/10.1175/1520-0469(1997)054<0072:AMFTBS>2.0.CO;2

771 Webster PJ, Magaña VO, Palmer TN et al (1998) Monsoons: processes, predictability, and the
772 prospects for prediction. J Geophys Res 103(C7):14451-14510.
773 https://doi.org/10.1029/97JC02719

774 Wei Y, Ren H (2022) Distinct MJOs under the two types of La Niña. J Geophys Res Atmos
775 127(23):e2022JD037646. https://doi.org/10.1029/2022JD037646

776 Wheeler MC, Hendon HH (2004) An all-season real-time multivariate MJO index:
777 development of an index for monitoring and prediction. Mon Weather Rev 132(8):1917-
778 1932. https://doi.org/10.1175/1520-0493(2004)132<1917:AARMMI>2.0.CO;2

779 Wilson EA, Gordon AL, Kim D (2013) Observations of the Madden-Julian Oscillation during
780 Indian Ocean Dipole events. J Geophys Res Atmos 118(6):2588-2599.
781 https://doi.org/10.1002/jgrd.50241

782 Wyrtki K (1987) Indonesian through flow and the associated pressure gradient. J Geophys Res
783 92(C12):12941-12946. https://doi.org/10.1029/JC092iC12p12941

784 Yang Y, Xie SP, Wu L et al (2015) Seasonality and predictability of the Indian Ocean dipole
785 mode: ENSO forcing and internal variability. J Climate 28(20):8021-8036.
786 https://doi.org/10.1175/JCLI-D-15-0078.1

787 Yeh SW, Cai W, Min SK et al (2018) ENSO atmospheric teleconnections and their response
788 to greenhouse gas forcing. Rev Geophys 56(1):185-206.
789 https://doi.org/10.1002/2017RG000568

790 Yoneyama K, Masumoto Y, Kuroda Y et al (2008) MISMO field experiment in the equatorial
791 Indian Ocean. Bull Am Meteorol Soc 89(12):1889-1903.
792 https://doi.org/10.1175/2008BAMS2519.1

793 Zhang C (2005) Madden-Julian oscillation. Rev Geophys 43:RG2003.
794 https://doi.org/10.1029/2004RG000158

795 Zhou L, Murtugudde R (2010) Influences of Madden-Julian Oscillations on the eastern Indian
796 Ocean and the Maritime Continent. Dyn Atmos Oceans 50(2):257-274.
797 https://doi.org/10.1016/j.dynatmoce.2009.12.003

798 Zhou L, Murtugudde R (2020) Oceanic impacts on MJOs detouring near the Maritime
799 Continent. J Climate 33(6):2371-2388. https://doi.org/10.1175/JCLI-D-19-0505.1

800

801

802

803